Relaxation of jammed colloidal suspensions after shear cessation

Francesca Ianni,[1,2,*] David Lasne,[1,3] Régis Sarcia,[1] and Pascal Hébraud[1,4]
[1]*P.P.M.D., UMR 7615 ESPCI, 10 rue Vauquelin 75231, Paris Cedex 05, France*
[2]*SOFT-INFM-CNR, c/o Università di Roma "La Sapienza," I-00185, Roma, Italy*
[3]*C.P.M.O.H., UMR 5798, 351 cours de la Libération, 33405 Talence, France*
[4]*IPCMS, UMR 7504, 23 rue du Loess 67034, Strasbourg Cedex 02, France*
(Received 5 December 2005; revised manuscript received 12 May 2006; published 20 July 2006)

The dynamics of heterogeneities in a shear thickening, concentrated colloidal suspension is investigated through speckle visibility spectroscopy, a dynamic light scattering technique recently introduced [P. K. Dixon and D. J. Durian, Phys. Rev. Lett. **90**, 184302 (2003)]. Formation of shear-induced heterogeneities is observed in the jamming regime, and their relaxation after shear cessation is monitored as a function of the applied shear stress. The relaxation time of these heterogeneities increases when a higher stress is applied.

DOI: 10.1103/PhysRevE.74.011401 PACS number(s): 83.80.Hj, 83.85.Ei, 42.25.Fx

INTRODUCTION

Concentrated colloidal suspensions exhibit complex rheological behavior. At low stress, their viscosity decreases with increasing stress, whereas it increases when the applied stress exceeds a critical value. The increase of the viscosity may even lead to cessation of the flow; the suspension jams [1]. The first phenomena, called shear thinning, has been extensively studied and is associated with the advent of a long range order between the particles, which align along the flow direction. On the contrary, the particle microstructure responsible for the shear-thickening phenomena at high stress is still not completely understood. The mechanism responsible for shear thickening has been studied numerically and theoretically in the simple shear geometry. In that case, the stress tensor exhibits a compression along an axis oriented at $3\pi/4$ from the flow direction in the flow-gradient plane. When the compressive force along this axis overcomes repulsive interparticle forces [2] (of Brownian, steric, or electrostatic origin), anisotropic clusters of particles, oriented along the compression axis, form. As a consequence, a rapid increase of the viscosity occurs [3–5]. This has the further effect of a sign reversal in the first normal stress difference, which takes negative values in strong shear flows [6]. The cluster formation is reversible [7] and, according to simple model, they may span over the entire gap of the system [8], thus leading to flow instability [1]. The size distribution of these shear-induced heterogeneities has been studied in [8] for a two-dimensional, simple driven diffusive model and a hysteresis is found in the evolution of their average size as a function of the shear rate. Numerical simulations of concentrated hard spheres under shear [9], taking hydrodynamic interactions into account, show that the probability of having a percolating cluster with a given interparticle spacing saturates when the applied stress increases. Moreover, the interparticle spacing inside a given cluster decreases when the applied stress increases.

Experimental study of the shear-induced heterogeneities is a challenging issue. The first measurements investigating the particle structure of a system in the shear-thickening regime were conducted through small angle neutron scattering [10] and proved the existence of a short range order and the absence of long range order. In this kind of experiments [11], the quiescent scattering profile was recovered after shear cessation, showing that the structure formed under shear is not of a permanent nature. On a mechanical point of view, the anisotropy of the particle pair distribution function results in nonzero values of the first and second normal stress differences. Nevertheless, measurements of normal stress differences are extremely difficult due to their very small value [12]. Thus, direct microscopic observations have been used to probe the heterogeneities of the suspension concentration [13,14]. Confocal microscopy enables the observation of index-matched suspensions of colloidal particles. It has been observed that just after the cessation of flow at high shear rates, local particle density is extremely heterogeneous and highly concentrated regions appear. In that particular case, crystallites form under flow and are supposed to be responsible for jamming [14,15], Nevertheless, confocal microscopy does not allow the observation of rapid motion of particles; thus, the dynamics of the particles under flow cannot be investigated through this technique.

On the contrary, diffusing wave spectroscopy (DWS), a light scattering technique, is adapted to very turbid systems [16] and allows the observation of the dynamics at very short time scales. When the sample is illuminated with a coherent light, multiple scattering occurs. Light propagation can be described by a random walk, whose transport mean free path, l^*, decreases when the turbidity increases. An interference pattern forms on any imaginary screen, in particular on the illuminated side of the cell (backscattering geometry), or on the opposite side (transmission geometry). The light intensity is spatially correlated over an area called speckle. Motion of the scatterers leads to a significant change in the phase of the scattered light, and hence to a change in the intensity of a single speckle. The particle dynamics can thus be investigated through the study of the temporal fluctuations of the scattered intensity on a single speckle spot. One generally quantifies these fluctuations by computing the intensity autocorrelation function, calculated as a time average. In our case, we are interested in the dynamics of the particles just after flow cessation. This is a nonstationary dynamics and

*Electronic address: francesca.ianni@phys.uniroma1.it

thus cannot be studied through a time average measurement. The multispeckle diffusive wave spectroscopy technique (MSDWS) has been introduced to overcome this limitation [17], as the intensity autocorrelation function is computed by averaging the intensity fluctuations over the pixels of a digital camera detector collecting the whole speckle pattern. Nevertheless, the temporal resolution is limited by the low frequency of the camera collected images. In our case, the characteristic time of the system dynamics is too small to be investigated through this technique.

In this work, we overcome these problems by using a recently introduced technique, the speckle visibility spectroscopy (SVS) [18], in order to investigate the relaxation of the particles after flow cessation. The principle of the measurement is the following: for a given exposure time, the faster the dynamics of the suspension, the more the speckle image is blurred and the less contrasted is the speckle image. Quantitatively, one computes the contrast of an image for a given exposure time as the variance of the intensity distribution across the pixels. If the dynamics is changing in the system, for an exposure time in the range of the system dynamical timescales, the contrast allows exploration of the variations in the particle dynamics [18]. The temporal resolution of this technique is of the order of the exposure duration, much smaller than the elapsed time between two successive images, and allows the study of our system dynamics. More specifically, we apply a high shear stress to our suspension, and, after a given time, stop the stress application. The suspension is continuously illuminated by a laser beam, and by following the contrast of the interference pattern, we study the particle dynamics under shear and after shear cessation.

SAMPLE PREPARATION AND SVS MEASUREMENTS

Water suspension of spherical silica particles of diameter 640 nm, synthesized according to the Stöber method [19], are studied. To reach more easily the jamming regime the particle surface is roughened; for a concentrated suspension, it has been shown that the increased interparticle contacts and friction increase the overall viscosity and induce jamming at smaller stresses than for smooth spheres [15,20]. In order to roughen the particle surface, sodium hydroxide, in a mass percentage of 19% with respect to the mass of silica, is added to the suspension, which is then left under stirring for 24 h. At basic *p*H, the silica slowly depolymerizes [21] and one gets rough particles of the same diameter. The mean square surface roughness of the particles was measured by atomic force microscopy and is 6.20 nm, whereas it is 0.68 nm for the particles before the attack at basic *p*H [20]. The suspension is then rinsed through centrifugation and redispersed in Millipore water, until *p*H becomes neutral. We then prepared a suspension of rough particles at a volume fraction of 0.37. The sample has an opaque white appearance, so we operate in a multiple scattering regime.

A stress controlled Carri-Med rheometer is used. The cell is a Couette cell with a rotating internal cylinder of 27.5 mm diameter and a fixed external Plexiglass cylinder of 30.0 mm diameter, which lets the laser beam pass through. When loaded into the cell, the sample is submitted to high shear rates. Before any measurement, it is presheared at a low shear rate, below the jamming transition. Then, once poured in the cell, the same sample is used in the whole experiment. A Spectra-Physics argon polarized laser beam, of wavelength $\lambda=514$ nm, is expanded and hits the sample with a Gaussian spot size of 6 mm, at an angle of $\pi/6$ from the normal direction of the outer cylinder surface. The light is then multiply scattered by the suspension and the backscattered light is collected in a direction perpendicular to the cell outer surface. The collection optics consists of a collimating lens that focuses diffused light onto a diaphragm, which selects a part of it. Finally, a Pulnix charge-coupled device (CCD) camera behind the diaphragm collects the speckle pattern. The camera device has 768×484 pixels and can collect the images at a frequency of $\nu=15$ Hz. It is interfaced to a PC provided with a National Instruments card, and the data are analyzed in real time using LAB WINDOWS. The diaphragm size can be changed in order to adjust the speckle size and thus the ratio of pixels to speckle areas [17]. As the light multiply scattered by the sample will be depolarized, a polarizer is added between
the lens and the diaphragm in order to minimize direct reflections. All the measurements were performed in backscattering geometry, the dynamics of the particles is thus probed in a volume defined by the section of the diaphragm ($\simeq$6 mm$\times$6 mm) and the photon penetration depth in the sample. Using a procedure described elsewhere [20], we measured the photon mean free path inside the suspension and obtained $l^*=93\pm4$ μm. According to DWS theory, the penetration depth in backscattering geometry is of the order of a few mean free paths [16]. We can thus estimate that the volume explored in one experiment is of the order of 6 mm$\times$6 mm$\times$0.2 mm. It thus contains 10^9 particles but represents a small fraction of the entire Couette cell, and in particular, its depth is approximately one-fifth of the gap.

As the particles move, the speckle pattern changes and large intensity fluctuations occur at each pixel; if the exposure time of the camera is long compared to the time scale of speckle fluctuations, the same average intensity will be recorded for each pixel. On the contrary, if the exposure time is shorter, the speckle pattern is visible. This is the principle underlying the SVS technique [18], and the key measurable quantity is the variance of the intensity across the pixels. More precisely, we calculate the so-called contrast

$$C(T)=\frac{\langle I_T^2\rangle_p}{\langle I_T\rangle_p^2},$$

where $\langle\cdots\rangle_p$ is an ensemble average over all the pixels and the intensity I_T is the pixel time-integrated intensity over the exposure duration T. For T much larger than the dynamical time scale of the system, the contrast is expected to be one, while in the opposite limit the expected value is two. From another point of view, keeping T fixed, the contrast will be close to two if the system dynamics is slow and approximately one if the dynamics is fast with respect to T. The exposure duration of the camera device can vary in the range 64 μs to 19 ms. When the exposure duration is varied, the

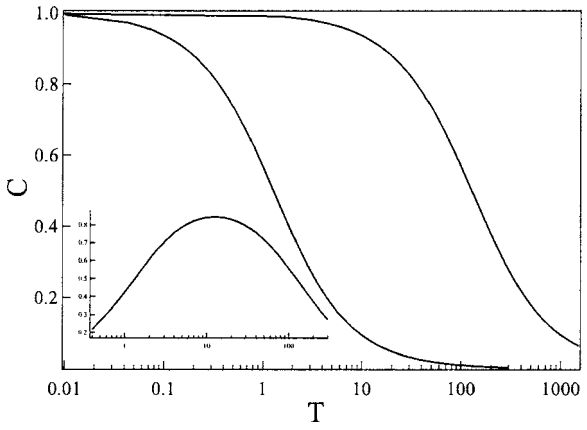

FIG. 1. Evolution of the contrast with the camera exposure duration T. The dynamics of the electric field correlation function g_1 is assumed to be described by a simple exponential with relaxation time τ_c. Continuous curve: $\tau_c=\tau_c^0=100$. Dashed curve: $\tau_c=\tau_c^1=1$. Inset: Difference between the two contrast curves, $C_{\tau_c^0}(T)-C_{\tau_c^1}(T)$ as a function of T. The maximum difference is obtained for a T value approximately equal to the geometric average of τ_c^0 and τ_c^1, $\sqrt{\tau_c^0\tau_c^1}$.

laser intensity is modified in order to keep $\langle I_T\rangle_p$, the average intensity over the pixels, fixed [22].

During an experiment, we chose to keep the exposure time constant. The optimum choice of the exposure time depends on the dynamics of the observed sample. Let us indeed assume that the dynamics of the system is characterized by a decorrelation time τ_c of the electric field autocorrelation function (g_1) [23] and that τ_c may take any value between τ_c^0 and τ_c^1, corresponding to two different values of the contrast, $C_{\tau_c^0}(T)$ and $C_{\tau_c^1}(T)$. Assuming that g_1 exhibits a simple monoexponential decay, the contrast can easily be calculated as a function of T [18]; it is plotted for the values $\tau_c^0=1$ and $\tau_c^1=100$ in Fig. 1. We wish to observe the maximum variation of the contrast during the experiment. One needs to find the value of T that maximizes the difference between $C_{\tau_c^0}(T)$ and $C_{\tau_c^1}(T)$. We observe that the maximum difference between the two curves is reached for a time $T=12$, of the order of the geometric mean of τ_c^0 and τ_c^1, $\sqrt{\tau_c^0\tau_c^1}$. This result can be easily generalized, as it does not change significantly if we model the electric field correlation function by other forms (different from a simple exponential), or if we consider a double decaying correlation function—with one time scale remaining fixed—to account for another dynamical process present in the system at a different time scale. We empirically chose for T the value that maximizes the variation of the contrast during the experiments and found that $T=5.08$ ms was the best choice for our system.

RESULTS AND DISCUSSION

The mechanical properties of the sample and the occurring of jamming are illustrated by the rheological measurement reported in Fig. 2, in which the sample undergoes a ramp of stress. For small stresses, the shear rate increases smoothly with the stress; then, when the stress reaches a

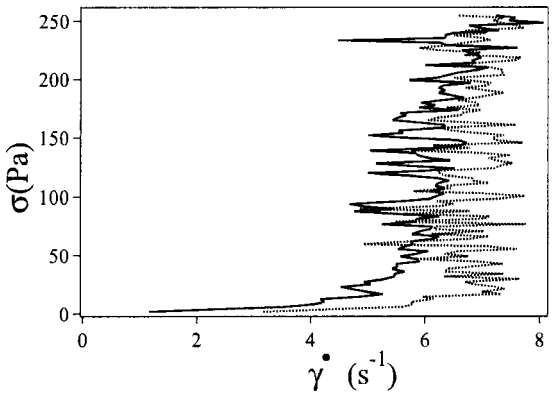

FIG. 2. Shear thickening of the concentrated suspension of rough silica particles. The volume fraction is $\phi=0.37$. Stress is controlled in Couette geometry and is increased from 0 Pa to 255 Pa at a rate of 2.1 Pa s^{-1} (continuous curve). Then the stress is decreased to zero with the same absolute rate (dashed curve). Shear thickening occurs for $\sigma\gtrsim 20$ Pa. A slight hysteresis is observed when the stress is decreased.

critical value, a transition occurs to a different regime, where the shear rate starts fluctuating around a fixed value. We will call this the shear jamming regime. If a decreasing ramp of stress is applied after the rising ramp, a slight hysteresis is observed in the stress vs shear rate curve.

Let us now apply a constant stress of 50 Pa above the jamming transition (Fig. 3). First, we observe that the shear rate is not stationary and exhibits huge fluctuations [1]. The observed contrast also fluctuates and its fluctuations are correlated to the shear rate fluctuations. When the sample is under shear, the faster and dominant movement of the particles is due to the flow. Assuming a linear shear rate, the typical time scale characterizing the scattered light intensity fluctuations is $\tau_s=\sqrt{10}/(\mathbf{k}_0 l^*)1/\dot{\gamma}$, where $\mathbf{k}_0=2\pi/\lambda$ is the laser beam wave vector, $\dot{\gamma}$ is the shear rate, and l^* is the photon transport mean free path in the medium [24]. So, when the flow velocity decreases due to the shear rate fluctuations in the jamming regime, as the particles move slower, the contrast will be higher and vice versa.

Under high stress values, the dynamics of the particles under shear may even be slower than the dynamics at rest. In

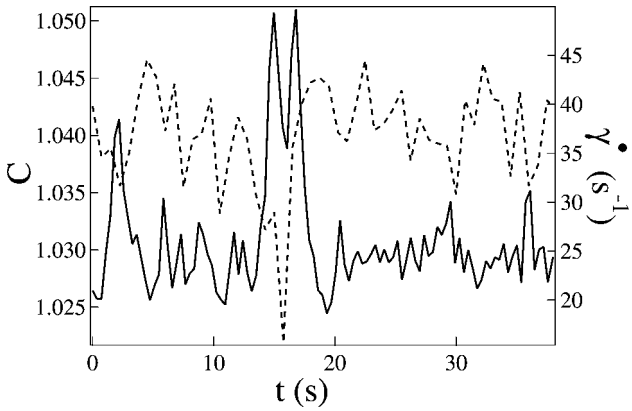

FIG. 3. Fluctuations of the gradient (dotted line) and the contrast (solid line) under an applied stress of 50 Pa. Low values of the gradient are associated to high values of the contrast.

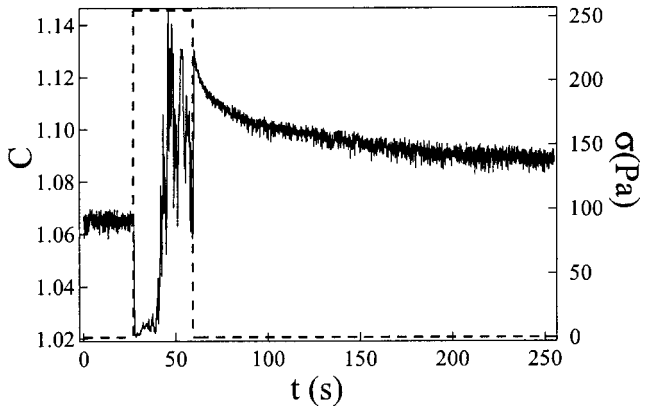

FIG. 4. Contrast behavior before, during, and after the application of a stress $\sigma=255$ Pa during 30 s. The stress history is plotted in a dashed line. During the stress application, strong contrast fluctuations are observed. After the shear cessation, the contrast exhibits an overshoot and then relaxes to a constant value.

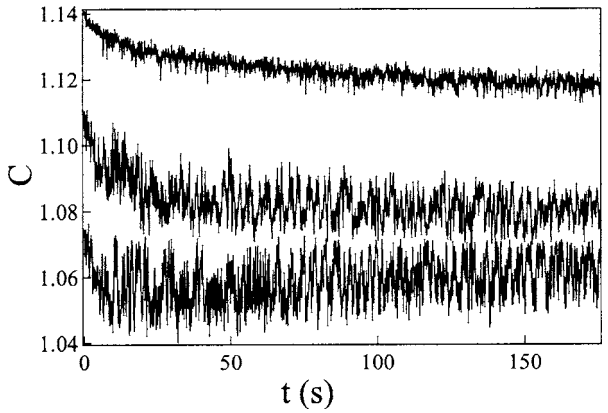

FIG. 5. Contrast relaxation, soon after application of a stress of $\sigma=180$ Pa during 30 s, for three different measurements performed under the same conditions. The measurements are highly nonreproducible. The overshoot of the contrast is not always observed, as exemplified by the bottom curve. The two other curves exhibit an overshoot, but its amplitude, its characteristic decorrelation time, the value of the baseline, and the noise of the contrast signal vary with the measurement.

Fig. 4 we report an experiment in which a high stress value in the jamming regime, $\sigma=255$ Pa, is applied for 30 s; then the application of stress is stopped. Before the shear, application the contrast at rest is equal to 1.06 and its relative noise, calculated as the standard deviation of the signal divided by its average value diminished by 1, is 4%. As soon as the stress is applied, the contrast drops to a smaller value of 1.02; then the suspension jams and huge contrast fluctuations occur. Remarkably, these fluctuations lead to contrast values higher than the contrast value at rest before or after the stress application. This means that during the shear, the particle drift velocity sometimes becomes so small that τ_s is not the dominant time scale anymore, so another dynamical time scale of the system can be revealed. Moreover, the dynamics characterized by this sometimes emerging time scale is slower than the dynamics of the system at rest. The particles thus organized themselves under flow in such a way that their motion is slower than their free motion at rest.

We now turn to the relaxation of the dynamics when the application of stress is stopped. We followed the evolution of the contrast after cessation of stress in the jamming regime. As soon as the stress application is stopped, we observe (Fig. 4) an overshoot of the contrast; just after stress cessation, the contrast value is much higher than the one at rest. It then slowly decreases to a constant value, which is not necessarily the same value it had before the shear. We observe that the contrast signal is very noisy. Let us, moreover, consider the noise amplitude along a relaxation curve (Fig. 4). Just after shear cessation ($60<t<80$ s), the amplitude of the fluctuations are smaller than after complete relaxation ($t>200$ s). This high value of the noise after relaxation of the dynamics of the suspension is a consequence of both the properties of the system and our choice of the shutter duration $T=5.08$ ms, which maximizes the amplitude of the contrast relaxation after shear cessation. Indeed, the contrast is very noisy if compared to the amplitude of the relaxation (Fig. 5). This prevents us from making systematic measurements with an easy quantitative analysis of the results. This noise is not due to the setup but is an intrinsic characteristic of the sample. This is shown in Fig. 6, where we plotted the contrast, measured for an exposure duration of the camera $T=19.1$ ms, for two samples at rest: the suspension of silica particles used in our work and a water solution of latex, taken as reference sample. The relative noise was calculated as previously explained. We obtained a value of 0.011 for the noise of the silica sample and of 0.0035 for the one of the reference sample, which is then a factor of three smaller. Besides, for a given sample, the noise of the contrast signal depends on the chosen T. The amplitude of the noise decreases when the exposure time T decreases with respect to the time scale of the system dynamics. Thus, the relative contrast noise for a silica suspension for $T=191$ μs is smaller by a factor of four than the noise for $T=19.1$ ms (Fig. 6). Nevertheless, as explained above, the value of T was chosen in order to maximize the contrast variation during the entire experiment. For that value ($T=5.08$ ms), the amplitude of the noise is similar to the amplitude measured at $T=19.1$ ms.

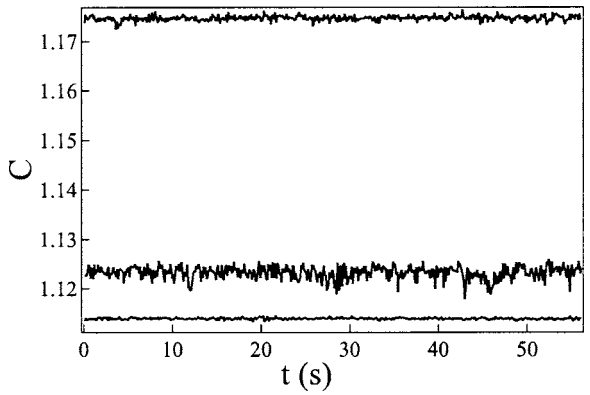

FIG. 6. Contrast evolution for a system at rest, for different samples and different camera exposure times T. From top to bottom: silica sphere suspension for $T=191$ μs, silica sphere suspension for $T=19.1$ ms, and water solution of latex for $T=19.1$ ms.

When the same measurement is repeated under the same conditions, the relaxation curve of the contrast exhibits scarce reproducibility (Fig. 5): its amplitude, its noise, the final value, and the characteristic relaxation time vary with the measure, while sometimes the overshoot cannot be observed either, as one of the three curves shows. In Fig. 4 we observed that once the stress application is stopped, the contrast plateau value after the relaxation is different from the contrast value at rest before stress application. Besides, Fig. 5 shows that this plateau value varies at each measurement. As the ensemble of measurements presented in Fig. 5 are taken with the same sample under the same conditions, it can be considered as a sampling in which a different region of the system after shear cessation is observed during each measurement. The presence of spatial heterogeneities in the system, consisting in slower and faster regions due to the very high concentration of the suspension, may be responsible for this lack of reproducibility. Indeed, if the length scale of this heterogeneity is of the order of the illuminated volume size, the nonreproducibility of the contrast value at rest may be easily explained. After each shear cessation and contrast relaxation, the illuminated region would be characterized by a different local concentration and then a different dynamical time scale inducing different contrast values.

Though the contrast signal is very noisy, we investigated qualitatively the dependence of the contrast relaxation behavior on the stress applied in the jamming regime. As the sample is heterogeneous, also the local shear rate may vary throughout the cell, but we can study the average trend of the contrast relaxation as a function of the applied stress. The evolution of the contrast after the shear cessation has been studied for three different applied stresses over the critical stress, and for each stress a set of eight measurements has been performed under the same conditions. The sample is first sheared under a constant stress of $\sigma \in \{100,180,255\}$ Pa for 30 s, and then stress application is ceased; the contrast value is recorded during the entire experiment. The curves which were not showing an overshoot have been dropped. We used the following criterium: we selected only the curves whose noise was smaller than the half-amplitude of the contrast decrease. The noise is measured as the standard deviation of the contrast when it reaches the final plateau value, i.e., when the noise is the highest. For the larger stress value, $\sigma=255$ Pa, none of the eight curves had to be dropped. For $\sigma=180$ Pa, two of the set were dropped and four for $\sigma=100$ Pa. In order to compare the relaxation times after the application of different stresses, we averaged the set of the remaining contrast data for each stress value. As the contrast relaxation has an exponential behavior, we applied a logarithmic binning procedure to each averaged curve in order to reduce noise at long times. First, the points of the curve were averaged in groups of ten, then they were further averaged in order to obtain a curve with 25 points logarithmically spaced on the x axis. The curves obtained from averaging the contrast evolution vs time after shear cessation for the three different stress values are plotted in Fig. 7, where, to be better compared, they have been normalized between 0 and 1. In order to quantify the relaxation time of these averaged curves, we have chosen a stretched exponential function $C(t)=\exp(-t/\pi)^{\beta}$, which

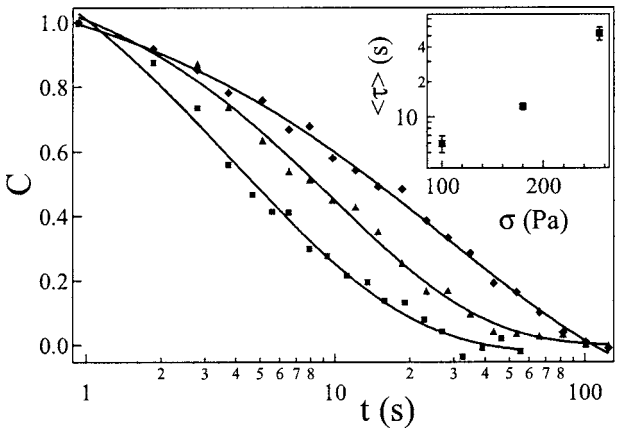

FIG. 7. Normalized and averaged contrast relaxation curves after the application of a constant stress σ during 30 s. Three values of the applied stress are studied: (■) $\sigma=100$ Pa, (▲)=180 Pa, and (◆)$\sigma=255$ Pa. Each curve is fitted with a stretched exponential form: $C(t)=e^{-(t/\tau)^{\beta}}$. Inset: Average relaxation time, $\bar{\tau}=\int_0^{\infty}\exp[-(t/\tau)^{\beta}]dt=\tau/\beta\ \Gamma(1/\beta)$ as a function of the applied stress.

gives a good fit of them. The value of the τ parameter varies between 4 s for the smaller stress and 29 s for the bigger stress. As the value of the β parameter does not remain constant but varies between 0.5 and 0.7, the average relaxation time $\langle\tau\rangle$ is calculated

$$\langle\tau\rangle=\int_0^{\infty}e^{-(t/\tau)^{\beta}}dt=\frac{\tau}{\beta}\Gamma\left(\frac{1}{\beta}\right), \tag{1}$$

where Γ is the Euler gamma function. The values of $\langle\tau\rangle$ are plotted as a function of the stress in the Fig. 7 inset. Thus, the higher the applied stress, the slower the contrast relaxation after shear cessation.

Dynamical heterogeneities must be associated to the formation of spatial structures under shear that relax when shear is stopped. Numerical simulations of concentrated colloids under shear [9] show that hydrodynamic clusters form. If similar behavior occurs in our system, as also indicated by confocal microscopy observations [15], spatial particle concentration heterogeneities develop under shear. Thus, denser regions may be responsible for slow particle dynamics. Nevertheless, our measurements do not allow description of the precise evolution of these heterogeneities as a function of the applied stress. It has been observed numerically that the distance between neighboring particles inside clusters decreases when the applied stress increases. One may thus assume that the volume fraction of particles inside the denser regions increases with the applied stress, thus favoring a slowing down of their relaxation after shear cessation. Nevertheless, also an increased volume fraction of these dense regions may be responsible for our results, as suggested by the fact that the higher the stress, the more frequently the contrast overshoot shows up in the illuminated volume. Further experiments should be made to clear up which of the two phenomena is responsible for the slowing down of the contrast relaxation for higher applied stress.

CONCLUSION

We investigated the flow-induced structure relaxation after shearing a suspension of concentrated silica particles in the jamming regime. These experiments thus lead to the following observations.

(i) Under shear, at some instants the dynamics of the particles is slower than their dynamics at rest (Fig. 4).

(ii) When the shear is stopped, the contrast relaxes back to a lower value, and contrast relaxation curves after shear cessation exhibit huge noise amplitude (Fig. 5).

(iii) The contrast relaxation time after shear cessation is an increasing function of the applied stress (Fig. 7).

These observations may be due to shear-induced spatial heterogeneities of the particle concentration. Numerical simulations suggest that several phenomena may be responsible for our results: the formation of denser regions and an increase of their volume fraction, or a decrease of the intercolloidal distance inside these regions [9] for an increasing applied shear stress. Further experiments and direct observation of the colloid organization under shear should allow determination of the correct interpretation.

ACKNOWLEDGMENTS

The authors wish to thank R. Di Leonardo and G. Ruocco for fruitful discussions.

[1] D. Lootens, H. Van Damme, and P. Hebraud, Phys. Rev. Lett. **90**, 178301 (2003).
[2] B. J. Maranzano and N. J. Wagner, J. Rheol. **45**, 1205 (2001).
[3] R. S. Farr, J. R. Melrose, and R. C. Ball, Phys. Rev. E **55**, 7203 (1997).
[4] P. Raiskinmaki, J. A. Astrom, M. Kataja, M. Latva-Kokko, A. Koponen, A. Jasberg, A. Shakib-Manesh, and J. Timonen, Phys. Rev. E **68**, 061403 (2003).
[5] J. Bergenholtz, J. F. Brady, and M. Vivic, J. Fluid Mech. **456**, 239 (2002).
[6] I. E. Zarraga, D. A. Hill, and D. T. Leighton, Jr., J. Rheol. **44**(2), 185 (2000).
[7] J. Bender and N. J. Wagner, J. Rheol. **40**, 899 (1996).
[8] O. J. O'Loan, M. R. Evans, and M. E. Cates, Physica A **258**, 109 (1998).
[9] R. C. Ball and J. R. Melrose, Adv. Colloid Interface Sci. **59**, 19 (1995).
[10] H. M. Laun, R. Bung, S. Hess, W. Loose, O. Hesse, K. Hahn, E. Hadicke, R. Hingmann, F. Schmidt, and P. Lindner, J. Rheol. **36**, 743 (1992).
[11] H. Watanabe, M-L. Yao, K. Osaki, T. Shikata, H. Niwa, Y. Morishima, N. P. Balsara, and H. Wang, Rheol. Acta **37**, 1 (1998).
[12] V. G. Kolli, E. J. Pollauff, and F. Gadala-Maria, J. Rheol. **46**, 321 (2002).
[13] M. D. Haw, Phys. Rev. Lett. **92**, 185506 (2004).
[14] P. Varadan and M. J. Solomon, J. Rheol. **47**, 943 (2003).
[15] D. Lootens, H. van Damme, Y. Hémar, and P. Hébraud, Phys. Rev. Lett. (to be published).
[16] D. J. Pine, D. A. Weitz, P. M. Chaikin, and E. Herbolzheimer, Phys. Rev. Lett. **60**, 1134 (1988).
[17] L. Cipelletti and D. A. Weitz, Rev. Sci. Instrum. **70**, 3214 (1999).
[18] P. K. Dixon and D. J. Durian, Phys. Rev. Lett. **90**, 184302 (2003).
[19] W. Stober and A. Fink, J. Colloid Interface Sci. **26**, 62 (1968).
[20] D. Lootens, Ph.D. thesis, Université Paris VI, 2004 (unpublished).
[21] R. K. Iler, *The Chemistry of Silica*, John Wiley, New York (1979).
[22] R. Bandyopadhyay, A. S. Gittings, S. S. Suh, P. K. Dixon, and D. J. Durian, e-print cond-mat/0506081.
[23] B. J. Berne and R. Pecora, *Dynamic Light Scattering*, Dover Publications, New York (1976).
[24] X. L. Wu, D. L. Pine, P. M. Chaikin, J. S. Huang, and D. A. Weitz, J. Opt. Soc. Am. B **7**, 15 (1990).